computation

MDPI

Article

Numerical Study on the Thermal Field and Heat Transfer Characteristics of a Hexagonal-Close-Packed Pebble Bed

Leisheng Chen [1,*], Jiahao Zhao [1], Yuejin Yuan [1] and Jaeyoung Lee [2]

[1] College of Electrical & Mechanical Engineering, Shaanxi University of Science & Technology, Xi'an 710021, China; 1905065@sust.edu.cn (J.Z.); yuanyj@sust.edu.cn (Y.Y.)
[2] School of Mechanical and Control Engineering, Handong Global University, Pohang 37554, Korea; jylee7@handong.edu
* Correspondence: lsheng.ch@sust.edu.cn; Tel.: +86-29-8613-2696

Abstract: Fuel elements in a high-temperature gas-cooled reactor (HTGR) core may be stacked with a hexagonal close-packed (HCP) structure; therefore, analyzing the temperature distribution and heat transfer efficiency in the HCP pebble bed is of great significance to the design and safety of HTGR cores. In this study, the heat transfer characteristics of an HCP pebble bed are studied using CFD. The thermal fields and convective heat transfer coefficients under different coolant inlet velocities are obtained, and the velocity fields in the gap areas are also analyzed in different planes. It is found that the strongest heat transfer is shown near the right vertices of the top and bottom spheres, while the weakest heat transfer takes place in areas near the contact points where no fluid flows over; in addition, the correlation of the overall heat transfer coefficient with the Reynolds number is proposed as $h_{avg} = 0.1545(k/L)Re^{0.8}$ ($Pr = 0.712$, $1.6 \times 10^4 \leq Re \leq 4 \times 10^4$). It is also found that the heat transfer intensity of the HCP structure is weaker than that of the face-centered-cubic structure. These findings provide a reference for reactor designers and will contribute to the development of safer pebble-bed cores.

Keywords: HCP-structured pebble beds; hotspots; heat transfer characteristics; simulation

Citation: Chen, L.; Zhao, J.; Yuan, Y.; Lee, J. Numerical Study on the Thermal Field and Heat Transfer Characteristics of a Hexagonal-Close-Packed Pebble Bed. *Computation* **2022**, *10*, 1. https://doi.org/10.3390/computation10010001

Academic Editors: Rachid Bennacer, Farid Bakir, Smaine Kouidri, Sang-Ho Suh and Ali Cemal Benim

Received: 4 November 2021
Accepted: 21 December 2021
Published: 5 January 2022

1. Introduction

The spherical fuel elements in a high-temperature gas-cooled reactor (HTGR) core are randomly packed [1], resulting in uneven heat transfer on the surface of the pebbles and hotspots being formed [2], which will affect the integrity of the fuel spheres and may cause serious accidents [3,4]. The formation of local hotspots is closely related to the porosity [5–7], the diameter of the pebble [8–10], and the flow state of the coolant in the pebble bed [11,12]. Analyzing the flow patterns, temperature distribution, and heat transfer efficiency in the pebble bed is of great significance to the design of high-temperature gas-cooled reactors and the safety of the reactor.

To study flow patterns of the coolant and thermo-hydraulic phenomena in the core, simplifying the random packing structure to a simple cubic (SC), face-centered cubic (FCC), or body-centered cubic (BCC) for analysis has been done by many experiments and simulations [13–15]. Lee et al. [16] performed numerical simulations on the treatment effects of the contact between the adjacent pebbles and concluded that the flow regimes and their relevant flow-induced local heat transfer were significantly dependent on the modeling of the inter-pebble region. Ahmadi et al. [17] simulated random, BCC, and FCC fixed beds and found that the pressure drop increased in this order. In addition, a new equation is concluded from the data, which is able to estimate the pressure drop of a packed bed for high particle Reynolds numbers, from 15,000 to 1,000,000. Li et al. [18] numerically studied the thermal–hydraulic characteristics of PBWR with a BCC structure and obtained the distributions of coolant temperature, velocity, pressure, and the Nusselt number. Hassan et al. [19,20] applied the large-eddy simulation (LES) and direct numerical

simulation (DNS) methods to analyze the fluid field in a BCC-structured pebble bed containing 147 pebbles. Fick et al. [21] used the FCC-structured pebble bed to simulate the flow with a Reynolds number of 9308 and cross-verified by using available quasi-direct numerical simulation (q-DNS) data. Shams et al. [22] conducted a quasi-direct numerical simulation (q-DNS) and large-eddy simulation (LES) on the flow field in a single FCC pebble bed. Those results were used to assess the predictions of the detached-eddy simulation (DES) and unsteady Reynolds-averaged Navier–Stokes (RANS) model computations. Atmakidis et al. [23] used computational fluid dynamics (CFD) to study the influence of confining walls on the pressure drop in regular (BCC and FCC structures) and irregular pebble beds. Numerical investigations of the regular configurations show strong channeling throughout the bed near the wall where the local void fraction is substantially high. The flow inside the packing is very slow. Dasgupta et al. [24] performed numerical simulations to study the velocity distributions and flow maldistributions in packed beds with SC packing and FCC packing. Jia et al. [25] studied the different effects of bed configuration on the flow characteristics of a pebble bed through a particle tracking velocity (PTV) experiment and suggested a new design of pebble bed configuration. Chen et al. [26] created a numerical simulation model and validated it by experiments. The flow field distribution of the fluid in the FCC structure pebble bed was obtained, and the stagnant flow zone and the fast flow zone were identified. To the best of our knowledge, the analysis of the fluid flow characteristics in the HCP-structured pebble bed has not been fully studied. Heat transfer analysis in different pebble beds was also performed by different research groups. Bu et al. [27] conducted a numerical study on the effective transfer coefficient (ETC) in an SC-structured pebble bed. It is found that natural convection has little influence on the solid pebble temperatures, but it would affect the fluid temperatures. Hu et al. [28] and Wang et al. [29] proposed that the use of grids in the pebble bed to fix the fuel spheres into a quasi-SC structure could increase the effective convection area in the pebble bed and, therefore, improve the heat transfer efficiency. The grid structure could indeed enhance the heat transfer in the orderly stacked pebble bed and reduce the pressure drop to a certain extent, but its heat transfer efficiency was not better than that of the randomly stacked pebble bed. Ferng et al. [30] compared the thermal fields of the BCC and FCC pebble beds and a higher heat transfer capability and lower pebble temperature were found in the FCC pebble bed. Song et al. [31] simplified the BCC and FCC models and calculated the pressure drop and the local average Nusselt number. Dave et al. [32] analyzed the heat transfer characteristics of the fluoride-salt-cooled high-temperature reactor (FHR) pebble bed and found that different lattice geometries (SC, BCC, FCC) have significant effects on the heat transfer characteristics. Chen et al. [33] analyzed the impact of heat transfer characteristics by inserting small pebbles into the FCC-structured pebble bed. The results showed that placing pebbles of different diameters (D = 0, 0.03, 0.04, and 0.05 m) in the voids of the pebble layer with a diameter of 12 cm could maximally increase the average heat transfer coefficient (HTC) by 28.8%. As stated above, these studies mainly focus on the analysis of heat transfer characteristics of SC, FCC, and BCC stacking structures, while research on a hexagonal-close-packed (HCP) pebble bed are scarcely conducted.

Given the possibility of pebbles stacked with an HCP structure in a pebble bed, it is necessary to study the heat transfer characteristics of the HCP pebble bed. Moreover, the HCP and FCC structures have the same packing ratio (or porosity as 0.26), which is much larger than that of BCC (porosity as 0.32) and SC (porosity as 0.476), and hotspots may be easily formed on the HCP pebbles as they are on FCC-structured pebbles. Furthermore, analysis of the HCP structure will help researchers build up a randomly packed bed more accurately (by mixing SC, BCC, FCC, and HCP with specific percentages), which partly lowers the difficulty of investigating local hotspots in a randomly packed bed. In this study, an HCP pebble bed is built, and heat transfer characteristics are investigated by a numerical method. The temperature fields, velocity fields, and convective heat transfer coefficients are obtained under different coolant inlet velocities. In addition, the correlations of the heat transfer coefficient and the Nusselt number with the Reynolds number are, respectively,

proposed. The heat transfer intensity is compared with that of the FCC structure. These findings not only provide references for future heat transfer enhancement of an HCP or randomly packed reactor cores but also for searching for an effective methodology that can be used to lower surface temperatures of pebbles in beds packed with any kind of structure and then reducing the possibility of forming local hotspots, which definitely makes contributions to a safer reactor design.

2. Numerical Methods

2.1. Geometry

As shown in Figure 1a, the geometric model consists of a fluid part (air) and a solid part (brass). The duct (170 mm × 170 mm × 600 mm) presents a hexagonal prism shape. Figure 1b,c, respectively, shows the solid and the fluid part. A unit cell of HCP lattice contains 7 atoms in both the top and bottom layers, and 3 atoms in the layer between; therefore, the solid part is composed of 17 pebbles and 17 heaters. For the convenience of thermal measurement and future flow visualization in the experiments, the pebbles were designed with a diameter of 120 mm; to ensure that the fluid is fully developed at the entrance region and does not flow back after flowing out of the test section, the duct length was determined to be 600 mm. In addition, the middle layer was arranged with three fuel spheres 120° apart. It is worth noting that the diameter of each contact point was set to 2 mm [16,26]. The relevant parameters of the components are listed in Table 1.

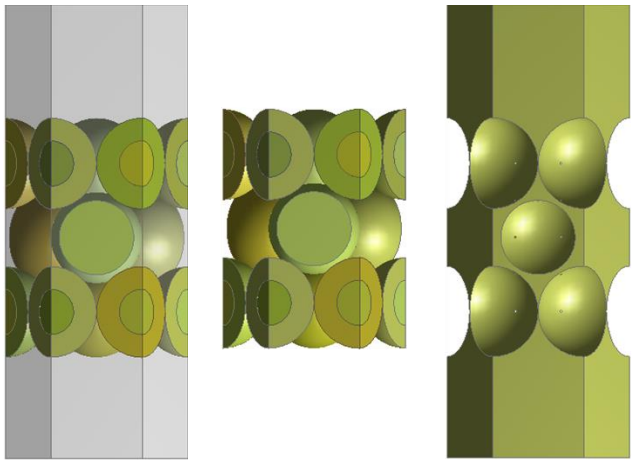

(**a**) (**b**) (**c**)

Figure 1. (**a**) Full geometry, (**b**) the solid part, and (**c**) the fluid part of the pebble bed.

Table 1. Properties of the materials used in the simulation.

Properties	Air (0.1 MPa, 298.15 K)	Brass [34]
Density (ρ) [kg/m^3]	1.1855	8700
Viscosity (μ) [Pas]	1.846×10^{-5}	-
Heat capacity (C_p) [J/kg/K]	1000	380
Thermal conductivity (k) [W/m/K]	0.02605	109
Characteristic (L) [m]	-	0.12

2.2. Meshing

In this study, the CFX-17.0 software was used to numerically simulate the HCP pebble bed, using unstructured grids to generate tetrahedral and hexahedral cells in the body domains (including the fluid domain and the solid domains) and the boundary layer, respectively. Figure 2a–d shows a high-quality grid of the fluid, the pebble, the solid interface, and the fluid–pebble interface. The mesh size of fluid, pebbles, and heaters was set to 2×10^{-3} m. Six boundary layers were applied to both sides of the fluid–pebble interface.

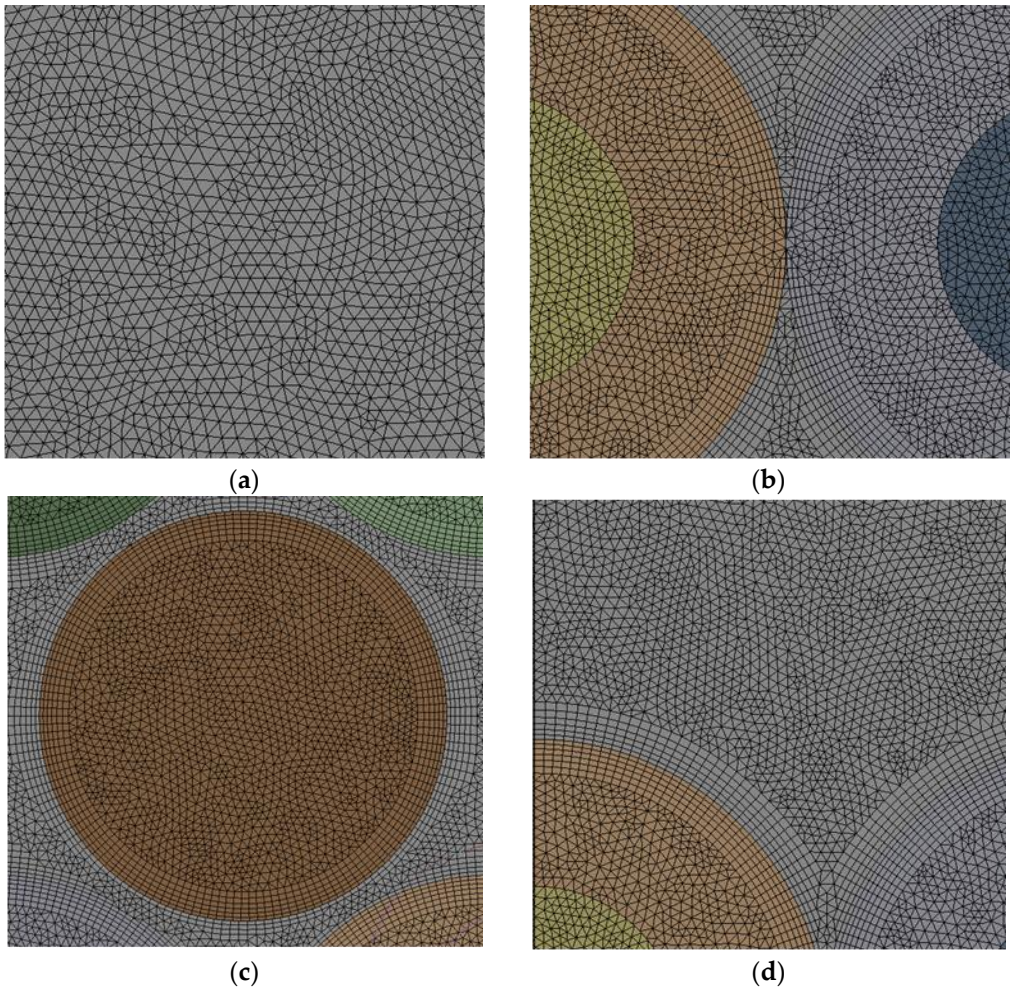

Figure 2. Meshes of (**a**) the fluid, (**b**) the pebble–pebble contact interface, (**c**) the pebbles, and (**d**) the fluid–solid interface.

The grid independence test was conducted, and four different grid sizes (1.5, 2, 2.5, and 3 mm) were selected. The temperature differences among the pebbles and between two cases were considered as the reference. The number of nodes and grids are shown in Table 2. Considering the surface temperature of the pebble, as shown in Figure 3a, the temperature difference among the pebbles in cases with mesh sizes of 3, 2.5, 2, and 1.5 mm was 8.7, 7.9, 7.4, and 7.3 K, respectively. In addition, as can be seen in Figure 3b, compared to the temperatures in the case of 1.5 mm, the maximum temperature difference for cases with a grid size of 2, 2.5, and 3 mm at the same measuring position was 0.5, 1.4, and 2.5 K, respectively. The mesh density had little impact on the surface temperature when comparing mesh sizes of 1.5 with 2 mm; however, the computation time was a few times more for the case of 1.5 mm. Lastly, the grid size was selected as 2 mm, and the total number of nodes and elements were around 4.62 million and 22.1 million, respectively.

Table 2. Elements' sizes and temperature differences.

Mesh Size [m]	Grid Number	Mesh Number	ΔT among Pebbles [K]	ΔT among Cases [K]
1.5×10^{-3}	10,595,737	53,059,477	7.3	-
2×10^{-3}	4,625,779	22,107,175	7.4	0.5
2.5×10^{-3}	2,442,427	11,241,689	7.9	1.4
3×10^{-3}	1,473,143	6,506,388	8.7	2.5

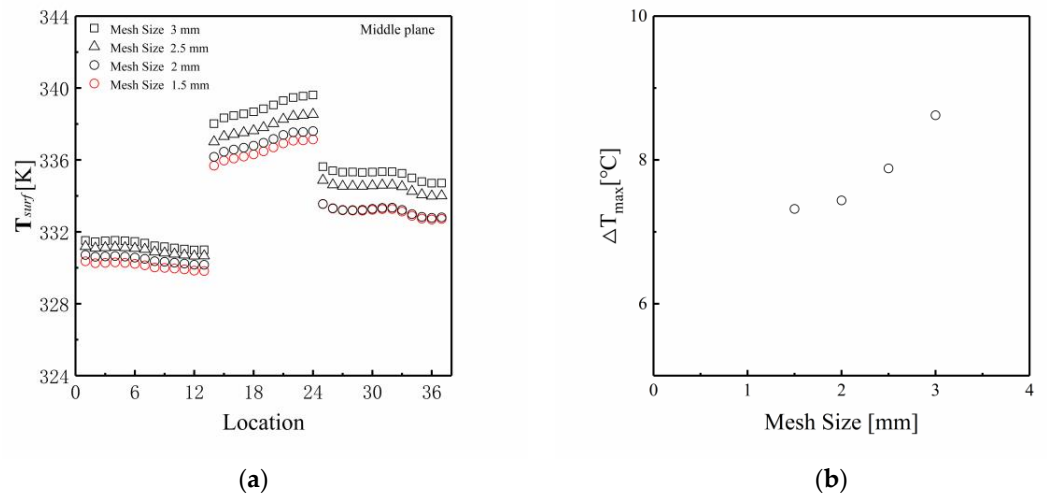

Figure 3. (**a**) Surface temperature of pebbles under four different mesh sizes; (**b**) maximum temperature difference.

2.3. Governing Equations and Boundary Conditions

The governing equations mainly include continuity (Equation (1)), momentum (Equation (2)), energy (Equation (3)), and the turbulence model, as shown below. It is worth noting that a standard k-ε turbulence model is used to describe the flow and heat transfer process in the pebble, since the k-ε model showed a smaller uncertainty than a k-ω or SST model did, and a DNS or LES method requires higher computational load. Particularly, the deviation of the HTC and surface temperatures obtained by simulation with the standard k-ε model was found to be not larger than 1.2% and 1.5% from that obtained by experiments [26].

$$\nabla \cdot (\rho U) = 0 \tag{1}$$

$$\nabla \cdot (\rho UU) = -\nabla p' + \nabla \cdot \left[\mu_{eff}\left(\nabla U + (\nabla U)^T\right)\right] + S_M \tag{2}$$

$$\nabla \cdot (\rho Uh) = \nabla \cdot \left(k_{eff}\nabla T\right) + S_E \tag{3}$$

$$\mu_{\mathrm{eff}} = \mu + C_\mu \rho \frac{k^2}{\varepsilon} \tag{4}$$

where p' is the modified pressure; μ_{eff}, the effective viscosity; C_μ is constant and has a value of 0.09; k and ε, respectively, come from the turbulence kinetic energy equation and turbulence dissipation rate equation; S_M, the sum of body forces, ignored in this simulation; h, the static enthalpy; k_{eff}, the effective thermal conductivity; and S_E includes the heat energy generated by the external heat sources, it can be neglected since no external heat source is employed.

For the boundary conditions, the inlet velocities were selected as 2.1, 2.8, 3.5, and 4.3 m/s, respectively, the inlet temperature was set as 298.15 K, and the required mass flow rate flowed in through the inlet. The turbulence intensity was 5%. The average static pressure at the outlet boundary was set to zero. Non-slip walls and thermal insulation materials were used for the walls around the fluid domain, and the surface of the pebble was also regarded as a non-slip wall. Radiation from these surfaces was also not taken into account due to the lower surface temperature. A power density of 1×10^6 W/m^3 was supplied to all heaters.

2.4. Solver Settings and Measurement Locations

The ANSYS default CFX-solver was used to compute all equations. For the solver control, the turbulence numerics and high-resolution advection schemes were selected to produce high-quality solutions that would reduce spatial discretization errors. The auto

timescale was chosen to allow the solver to use an internally calculated physical timescale based on the domain geometry, physics, flow conditions, and boundary conditions, and the timescale factor was set to 1.0, RMS for the residual type. The convergence was considered to be achieved when the residuals reached 10^{-4} for continuity, momentum, turbulent dissipation rate, and turbulent kinetic energy, whereas it had to reach 10^{-5} for the energy equation. The maximum iterations were 1000 for each computation.

As shown in Figure 4a,b, the middle plane (blue) and diagonal plane (gray) were selected to study the local heat transfer phenomenon in an HCP-stacking bed. For this purpose, we marked 37 and 20 measuring points on the surface of a few pebbles in the middle plane and diagonal plane, respectively, as shown in Figure 4c,d. In addition, to avoid pebble–pebble contact points, the directions of measuring lines 1, 13, 14, 24, 26, and 37 in the middle plane and measuring lines 10 and 20 in the diagonal plane were shifted by 2°, because the heat transfer at these points is determined by conduction rather than convection.

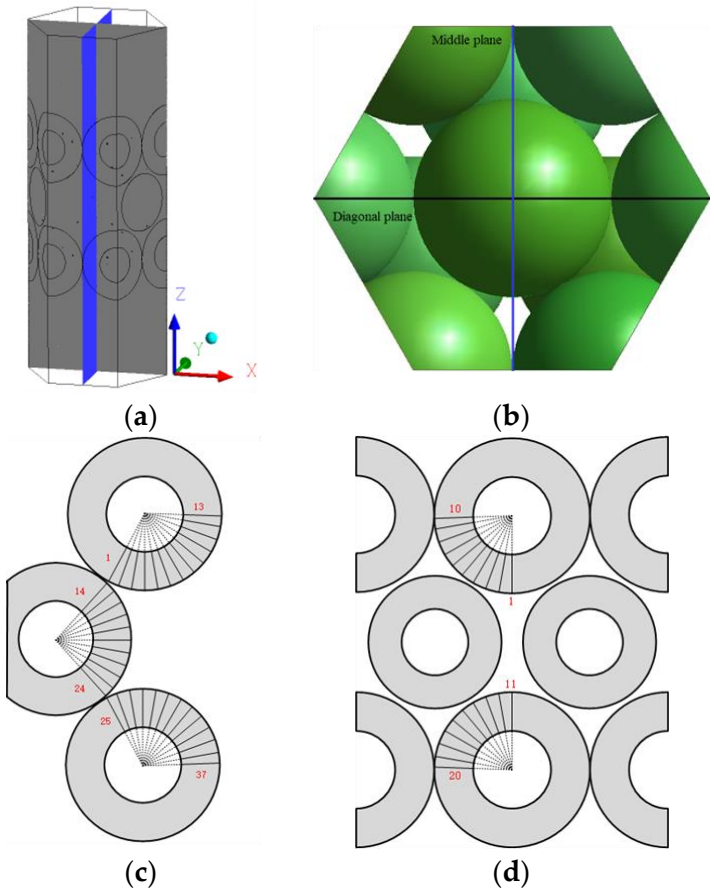

Figure 4. (**a**) The middle plane (blue)and the diagonal plane (gray); (**b**) the top view of relative positions of two designated planes; (**c**) measurement locations on the middle plane; (**d**) measurement locations on the diagonal plane.

3. Modeling and Analysis

3.1. Thermal Field and Flow Field

The flow and thermal fields under the inlet velocities of 2.1, 2.8, 3.5, and 4.3 m/s were investigated. Since the flow patterns in the HCP pebble bed were not changed, the variation trends of temperature were supposed to be similar for all cases. Therefore, the temperature field and velocity field were firstly analyzed when the inlet velocity was 2.1 m/s, and corresponding results are shown in Figures 5 and 6.

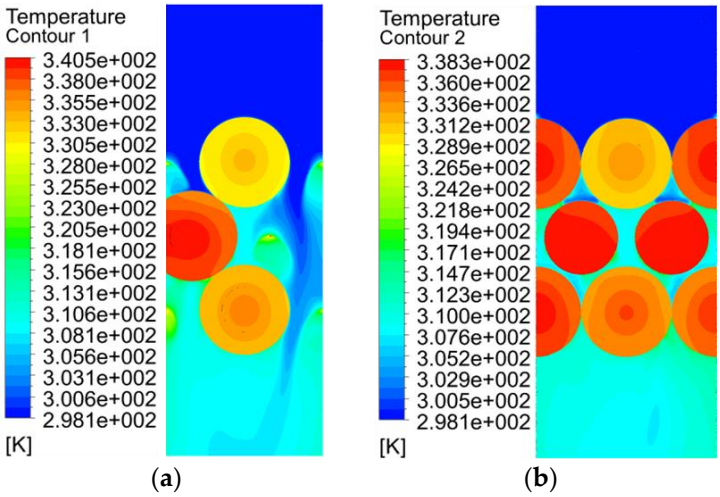

Figure 5. The temperature field of the pebble at (**a**) the middle plane and (**b**) the diagonal plane.

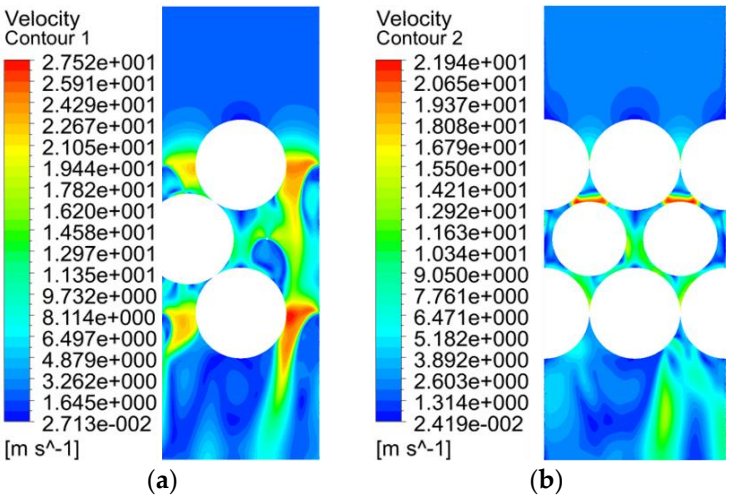

Figure 6. The velocity field of the pebble at (**a**) the middle plane and (**b**) the diagonal plane.

As shown in Figure 5a, among three designated pebbles, the middle pebble showed relatively higher pebble temperature while the upper pebble showed relatively lower temperature; furthermore, the same results can be seen in Figure 5b, which exhibits the thermal field of the diagonal plane. The coolant flows downward, and its temperature keeps increasing from the inlet to the outlet; therefore, the upper pebble is cooled down the most. Nevertheless, compared to the flow field in an HCP structure, the flow pattern in an FCC-structured bed is more complex [33]. It can be seen from Figure 6a,b that stagnation regions were formed at the rear area of the upper pebble, before the lower pebble, and measuring locations No. 8, 30 were in the middle plane as well, consequently, the local surface temperatures near these areas were predictably higher. Moreover, fast-flowing areas were formed near the left and right sides of both the upper and the lower pebbles in Figure 6a, due to a higher flow velocity leading to a better heat transfer, and therefore, corresponding local surface temperatures near these areas were lower. Fast-flowing areas (red regions) were found in front of middle pebbles as shown in Figure 6b, which will cause lower temperatures near the top of the middle pebbles than those at other places of the surface. It is believed that boundary layer separation will occur anywhere where the contact point/region is formed. This separation enhances the local heat transfer in the region near the contact point for certain cases, but it deteriorates the heat transfer for some other cases. An extended k-ε turbulence model might not only help to obtain a more accurate flow field since the structure is quite complicated [35] but also help to

differentiate heat power transferred by convection from heat transferred by conduction. Therefore, it is worth substituting the turbulence model with the extended k-ε model in the future simulations.

3.2. Pebble Surface Temperature

To understand the heat transfer characteristics of the HCP structure more clearly, the surface temperature of the pebble in the middle and the diagonal planes was studied and the results are shown in Figure 7a,b. Taking the case with an inlet velocity of 2.1 m/s, for example, it is found that the middle pebble had the highest surface temperatures among three designated pebbles, while the upper pebble had the lowest temperatures. Moreover, for the middle plane (Figure 7a), the temperatures of positions from No. 4 to No. 13 on the upper pebble surface and of positions from No. 31 to No. 37 on the lower pebble surface decreased gradually; such a trend can be explained by above-mentioned flow field. Furthermore, the temperatures of positions from No. 14 to No. 24 on the middle pebble surface were found to increase gradually. This is because the top pebble has relatively lower temperatures than the bottom one, and therefore, the temperature near the contact point formed between the middle and top pebbles will be lower due to conductive heat transfer. As the coolant flows and temperature increases, heat transfer between the middle pebble and the fluid becomes weaker, leading to a temperature-increasing trend. Temperature variation of the top and bottom pebbles at the diagonal plane was pretty small (Figure 7b); however, positions No. 7 and No. 18 had relatively lower temperatures in each pebble.

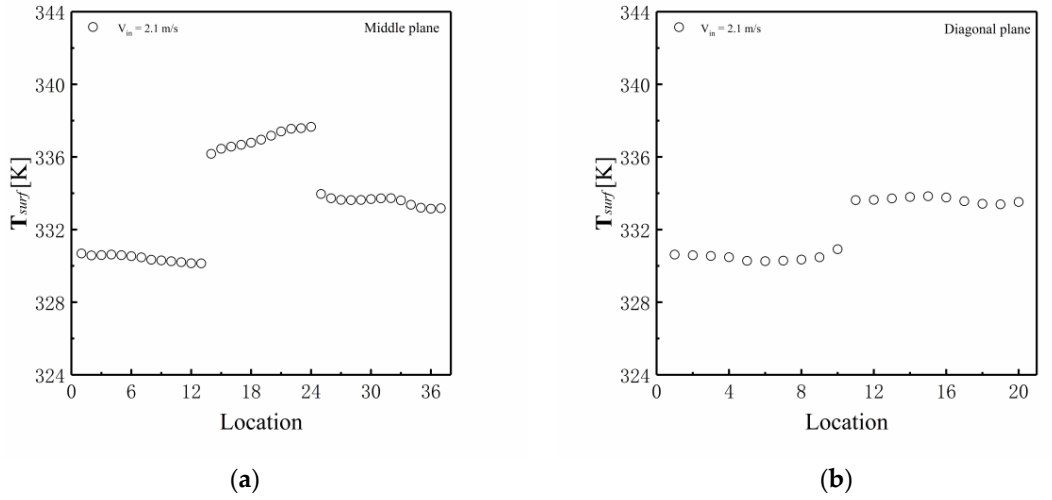

Figure 7. Pebble surface temperature under an inlet velocity of 2.1 m/s at (**a**) the middle plane and (**b**) the diagonal plane.

It was found that pebble temperatures at both the middle and diagonal planes under the other three cases (inlet velocities of 2.8, 3.5, and 4.3 m/s) had similar varying trends as shown in Figure 8a,b. However, as the coolant inlet velocity became larger, the surface temperatures decreased continuously. The maximum temperature difference among the three pebbles for all cases was 7.4, 5.9, 4.8, and 4.1 K, respectively.

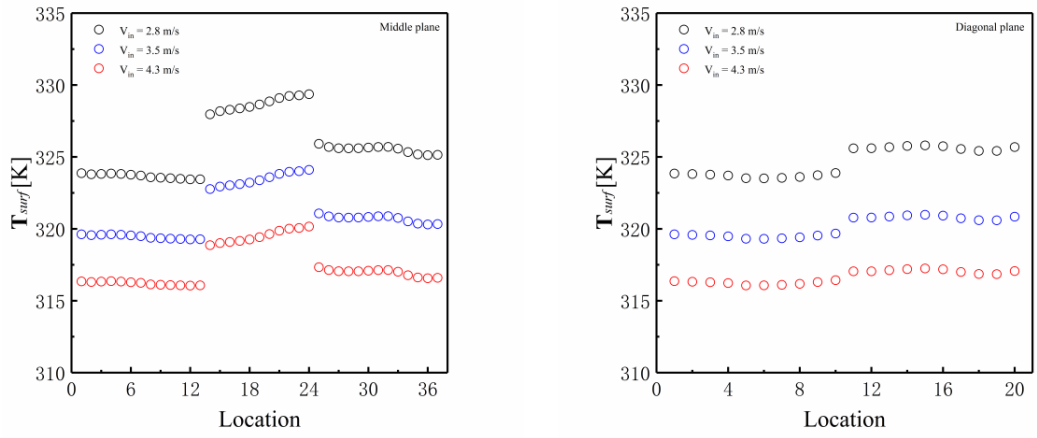

(**a**) (**b**)

Figure 8. The surface temperature of the pebbles under three other inlet velocities at the (**a**) middle plane and (**b**) the diagonal plane.

3.3. Local Heat Transfer Coefficient

The temperatures of a total of 57 measurement locations at the pebble surfaces and 5 mm beneath were measured to calculate the local HTCs according to Equation (5). The local HTCs could be used to characterize the local heat transfer intensity at the pebble surface.

$$\frac{k\Delta T_i}{r^2\left(\frac{1}{r_2}-\frac{1}{r_1}\right)} = h_i\left(T_{surf-i}-T_\infty\right) \tag{5}$$

where k is thermal conductivity; ΔT_i, the temperature difference between that at the pebble surface and that at 5 mm beneath at the *ith* measurement point, T_{surf}, the surface temperature of the pebble; and T_∞, the fluid temperature at the inlet; r, r_1, and r_2 are the radius of the pebble, distance from pebble center to the surface, and distance from pebble center to 5 mm beneath the surface, respectively.

The varying trend of local HTC at an inlet velocity of 2.1 m/s is shown in Figure 9a,b. For the middle plane (Figure 9a), the local heat transfer of the upper pebble became stronger and stronger from the bottom vertex to the right vertex (positions 4 to 13); the heat transfer firstly gets weaker at the middle pebble from positions 14 to 22, and then is strengthened a bit; as for the bottom pebble, the local HTC increased from positions 25 to 28 and decreased thereafter until position 32, then, it increased till the end. For the diagonal plane (Figure 9b), the local HTC at the upper pebble firstly increased from positions 1 to 6 and then decreased until position 10; while it firstly decreased from positions 11 to 15 and increased thereafter till position 18, and then decreased again. Such trends can be explained by the thermal and velocity fields described above. A higher coolant velocity near the pebble surface lowers the temperature and reduces the temperature difference between the pebble and the fluid; therefore, local heat transfer at the corresponding positions is enhanced.

Similar varying trends of local HTCs at both the middle and diagonal planes were found for the other three cases as shown in Figure 10a,b. The black, blue, and red circles represent the case with an inlet velocity of 2.8, 3.5, and 4.3 m/s, respectively. The local HTC increased as the inlet velocity got larger.

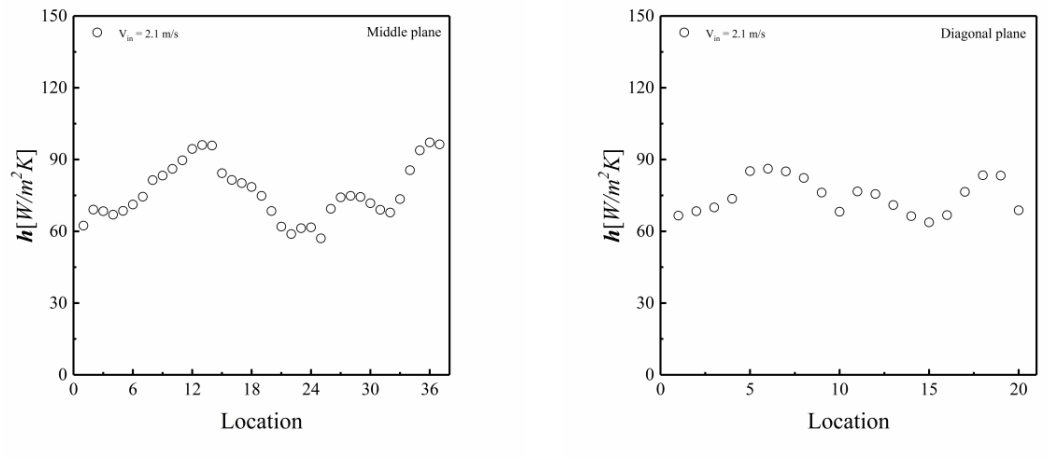

Figure 9. Local HTCs at inlet velocity of 2.1 m/s in (**a**) the middle plane and (**b**) the diagonal plane.

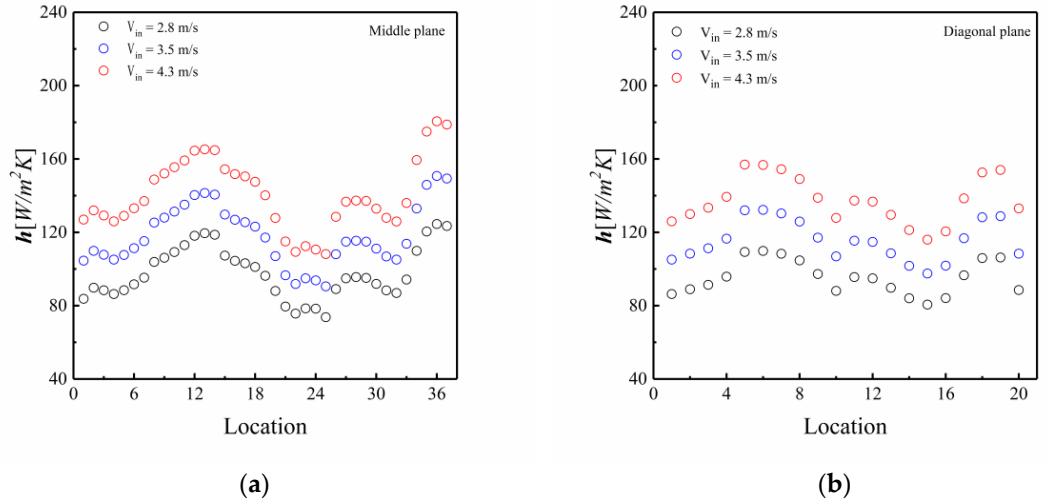

Figure 10. Local HTCs of three other cases in (**a**) the middle plane and (**b**) the diagonal plane.

3.4. Heat Transfer Characteristics

According to Equation (6), the average heat transfer coefficients of all four cases (the corresponding Reynolds numbers were 1.61×10^4, 2.15×10^4, 2.69×10^4, and 3.30×10^4, respectively) were computed and the results are represented by the circles in Figure 11. They are correlated with the Reynolds number and the correlation is proposed as Equation (7):

$$h_{avg} = \sum_{i=1}^{57} \left(\frac{k_{solid} \Delta T_i}{r^2 \left(\frac{1}{r_2} - \frac{1}{r_1} \right)} \times \frac{1}{T_{surf} - T_\infty} \times \frac{1}{57} \right) \left(W/m^2 K \right) \tag{6}$$

$$h_{avg} = 0.1545(k/L)Re^{0.8} \tag{7}$$

Furthermore, a correlation of the average HTC of the FCC-structured bed is plotted as the dotted line [8] in Figure 11 to compare with the heat transfer characteristics in the HCP pebble bed. It was found that the average HTC of the FCC pebble bed was higher. According to the correlation presented by KTA [36], the HCP pebble bed is supposed to have the same average HTC as the FCC pebble bed since they have the same packing ratio. This particular result might be explained by a less complexity of flow pattern in the HCP pebble bed, however, it might also be caused by not enough measurement locations; therefore, more efforts should be put on developing more measurement positions on representative

planes in the next-step work so that the distribution of the hotspots may be uncovered more precisely.

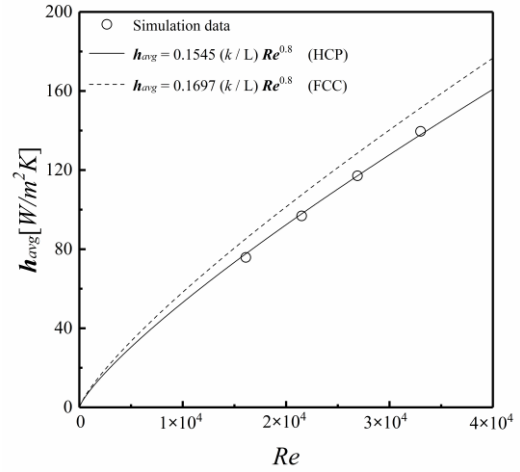

Figure 11. Correlation of average heat transfer coefficient with the Reynolds number.

For all cases, the Nusselt number was calculated using Equation (8) and the correlation between the Nusselt number and Reynolds number and Prandtl number is proposed as Equation (9). Such correlation is plotted in Figure 12.

$$\overline{Nu} = \frac{\overline{h}L}{k_{air}} \tag{8}$$

$$Nu = 0.177Re^{0.8}Pr^{0.4}\ (Pr = 0.712,\ 1.6 \times 10^4 \leq Re \leq 4 \times 10^4) \tag{9}$$

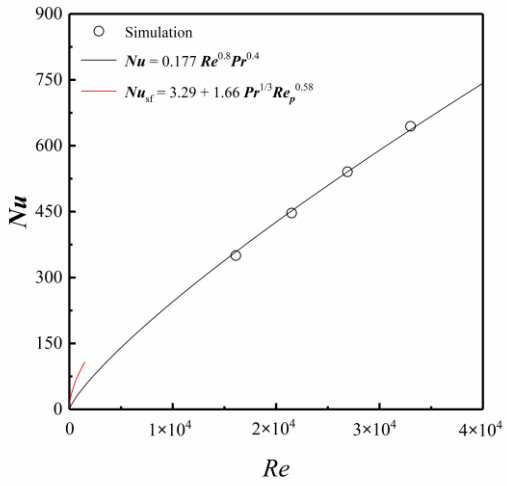

Figure 12. Correlation of the Nusselt number and comparison with other correlations.

Yang et al. [37] studied the heat transfer of an HCP pebble bed when the Reynolds number was less than 1500, and the correlation of the Nusselt number is plotted as a red line in Figure 12. It was found that the Nusselt number of an HCP structure is significantly greater than that of an FCC-packing structure. However, when the Reynolds number was larger than 1.61×10^4, an FCC pebble-bed had better heat transferability. It is believed that the flow regime plays a very important role in strengthening or weakening heat transfer in the pebble bed with different packing structures; moreover, the heat transfer of an HCP pebble-bed will be enhanced in laminar flow region while that of an FCC pebble-bed will be enhanced in turbulent flow region. More detailed comparisons on thermal and flow fields

between two structures are being conducted, and the results are expected to be reported very soon.

4. Conclusions

The CFX-17.0 was used to analyze the heat transfer characteristics of the HCP pebble bed to do the preparations for the next-step work of identifying the location of high-temperature hotspots in the core. Toward this end, the HCP numerical model was created and verified; in addition, the temperature and velocity fields of the pebble bed were analyzed on different planes. Furthermore, the local and average HTCs of the pebble were studied under different air inlet velocities. The main findings of this work are as follows:

1. The strongest heat transfer was found near the right vertices (positions 13 and 37) of the top and bottom pebbles.
2. The correlations of average HTC and Nusselt number were respectively proposed as $h_{avg} = 0.1545(k/L)Re^{0.8}$ and $Nu = 0.177Re^{0.8}Pr^{0.4}$ ($Pr = 0.712$, $1.6 \times 10^4 \leq Re \leq 4 \times 10^4$).
3. The average HTCs of the FCC-structured pebble bed were found to be higher than that of the HCP-structured pebble bed.

These findings are expected to provide a better understanding of the thermodynamics of the structured pebble bed and help to design the reactor core more safely. Future work will be focused on the following issues: (1) analyzing thermal field on pebble surfaces more comprehensively by setting up more measurement locations and identifying the hotspots' distribution; (2) enhancing heat transfer in the HCP pebble bed by adding small spheres, and studying the impact of number and size of small spheres on the heat transfer characteristics; (3) substituting the standard k-ε turbulence model with an extended k-ε model and analyzing the flow and thermal fields in the HCP pebble bed; (4) conducting experiments on surface temperature measurement and flow pattern visualization to validate numerical results.

Author Contributions: Conceptualization, L.C. and J.L.; methodology, L.C.; software, J.Z.; validation, J.Z. and L.C.; formal analysis, J.Z., Y.Y. and L.C.; investigation, Y.Y.; resources, J.L.; writing—original draft preparation, J.Z.; writing—review and editing, L.C.; supervision, Y.Y.; project administration, L.C.; funding acquisition, L.C. and J.L. All authors have read and agreed to the published version of the manuscript.

Funding: This work was supported by a start-up young researchers fund (2019-BJ07) granted by Shaanxi University of Science and Technology, China Postdoctoral Science Foundation (no. 2021M691999), and a National Research Foundation of Korea (NRF) grant funded by the Korea Government (MSIP) (Grant no. 2017M2A8A4018624).

Data Availability Statement: Data sharing is not applicable to this article.

Conflicts of Interest: The authors declare no conflict of interest.

Nomenclature

The following nomenclatures are used in this manuscript:

Symbols	Descriptions
C_μ	Constant
C_p	Heat capacity (J/Kg/°C)
D	Characteristic length of the pebble in the reactor core (m)
h	Heat transfer coefficient (W/m^{2}K)
k	Thermal conductivity (W/m/K)
L	Characteristic length of the pebble in the test section (m)
p'	Modified pressure (Pa)
r_1, r_2	Distance of thermocouple 1 and 2 from the pebble center (m)
S_E	Heat energy generated by external heat sources
S_M	Sum of body force
T_∞	Temperature of the coolant (K)

U	Velocity (m/s)
Δ	Difference
ε	Turbulence dissipation rate
μ	Viscosity (Pas)
ρ	Density (Kg/m^3)
∇	Gradient
Abbreviations	**Descriptions**
avg	Average
BCC	Body-centered cubic
CFD	Computational fluid dynamics method
DES	Detached-eddy simulation
DNS	Direct numerical simulation
ETC	Effective transfer coefficient
FCC	Face-centered cubic
FHR	Fluoride-salt-cooled high-temperature reactor
HCP	Hexagonal close-packed
HTC	Heat transfer coefficient
HTGR	High-temperature gas-cooled reactor
LES	Large-eddy simulation
PBWR	Pebble-bed water cooled reactor
PTV	Particle tracking velocity
q-DNS	quasi-direct numerical simulation
RANS	Reynolds-averaged Navier–Stokes
SC	Simple cubic
Surf	Surface

References

1. Zhang, Z.; Dong, Y.; Li, F.; Zhang, Z.; Wang, H.; Huang, X.; Li, H.; Liu, B.; Wu, X.; Wang, H.; et al. The Shandong Shidao Bay 200 MW e High-Temperature Gas-Cooled Reactor Pebble-Bed Module (HTR-PM) Demonstration Power Plant: An Engineering and Technological Innovation. *Engineering* **2016**, *2*, 112–118. [CrossRef]
2. Chen, L.; Lee, J. Experimental analysis of the thermal field and heat transfer characteristics of a pebble-bed core in a high-temperature gas-cooled reactor. *Ann. Nucl. Energy* **2017**, *110*, 338–348. [CrossRef]
3. Moormann, R. A Safety re-evaluation of the AVR pebble bed reactor operation and its consequences for future HTR concepts. In Proceedings of the Fourth International Topical Meeting on High Temperature Reactor Technology, Washington, DC, USA, 28 September–1 October 2008; pp. 265–274.
4. Moormann, R.; Kemp, R.S.; Li, J. Caution is needed in operating and managing the waste of new pebble-bed nuclear reactors. *Joule* **2018**, *2*, 1911–1914. [CrossRef]
5. Cheng, G.; Gan, J.; Xu, D.; Yu, A. Evaluation of effective thermal conductivity in random packed bed: Heat transfer through fluid voids and effect of packing structure. *Powder Technol.* **2020**, *361*, 326–336. [CrossRef]
6. Ren, H.; Liu, Y. Experimental investigation of fluid flow and heat transfer characteristics of a longitudinal corrugated liner for a combustion chamber. *Appl. Therm. Eng.* **2016**, *108*, 1066–1075. [CrossRef]
7. Zhu, Q.; Xuan, Y. Pore scale numerical simulation of heat transfer and flow in porous volumetric solar receivers. *Appl. Therm. Eng.* **2017**, *120*, 150–159. [CrossRef]
8. Chen, L.; Lee, J. Effect of pebble diameters on the heat transfer characteristics of a structured pebble bed in an HTGR. *Energy* **2020**, *212*, 118642. [CrossRef]
9. Latifi, M.S.; Colangelo, G.; Starace, G. A CFD study on the effect of size of fuel sphere on PBR core. *Exp. Comput. Multiph. Flow* **2019**, *2*, 109–114. [CrossRef]
10. Wu, Z.; Wu, Y.; Wang, C.; Tang, S.; Liu, D.; Qiu, S.; Su, G.; Tian, W. Experimental and numerical study on helium flow characteristics in randomly packed pebble bed. *Ann. Nucl. Energy* **2019**, *128*, 268–277. [CrossRef]
11. Shams, A.; Roelofs, F.; Komen, E.; Baglietto, E. Optimization of a pebble bed configuration for quasi-direct numerical simulation. *Nucl. Eng. Des.* **2012**, *242*, 331–340. [CrossRef]
12. Wu, C.; Ferng, Y.; Chieng, C.; Liu, C. Investigating the advantages and disadvantages of realistic approach and porous approach for closely packed pebbles in CFD simulation. *Nucl. Eng. Des.* **2010**, *240*, 1151–1159. [CrossRef]
13. Bu, S.; Yang, J.; Dong, Q.; Wang, Q. Experimental study of flow transitions in structured packed beds of spheres with electrochemical technique. *Exp. Therm. Fluid Sci.* **2015**, *60*, 106–114. [CrossRef]
14. Kim, M.-H.; Lim, H.-S.; Lee, W.J. Computational Fluid Dynamics Assessment of the Local Hot Core Temperature in a Pebble-Bed Type Very High Temperature Reactor. *J. Eng. Gas Turbines Power* **2009**, *131*, 012905. [CrossRef]
15. Li, L.; Yan, X.; Yang, J.; Wang, Q. Numerical investigation on band-broadening characteristics of an ordered packed bed with novel particles. *Appl. Energy* **2017**, *185*, 2168–2180. [CrossRef]

16. Lee, J.-J.; Park, G.-C.; Kim, K.-Y.; Lee, W.-J. Numerical treatment of pebble contact in the flow and heat transfer analysis of a pebble bed reactor core. *Nucl. Eng. Des.* **2007**, *237*, 2183–2196. [CrossRef]
17. Ahmadi, S.; Sefidvash, F. Study of pressure drop in fixed bed reactor using a computational fluid dynamics (CFD) code. *ChemEngineering* **2018**, *2*, 14. [CrossRef]
18. Li, H.; Qiu, S.; Zhang, Y.; Su, G.; Tian, W. Thermal hydraulic investigations with different fuel diameters of pebble bed water cooled reactor in CFD simulation. *Ann. Nucl. Energy* **2012**, *42*, 135–147. [CrossRef]
19. Hassan, Y.A. Large eddy simulation in pebble bed gas cooled core reactors. *Nucl. Eng. Des.* **2008**, *238*, 530–537. [CrossRef]
20. Yildiz, M.A.; Botha, G.; Yuan, H.; Merzari, E.; Kurwitz, R.C.; Hassan, Y.A. Direct numerical simulation of the flow through a randomly packed pebble bed. *J. Fluids Eng.* **2020**, *142*, 041405. [CrossRef]
21. Fick, L.H.; Merzari, E.; Hassan, Y.A. Direct numerical simulation of pebble bed flows: Database development and investigation of low-frequency temporal instabilities. *J. Fluids Eng.* **2017**, *139*, 051301. [CrossRef]
22. Shams, A.; Roelofs, F.; Komen, E.; Baglietto, E. Numerical simulation of nuclear pebble bed configurations. *Nucl. Eng. Des.* **2015**, *290*, 51–64. [CrossRef]
23. Atmakidis, T.; Kenig, E.Y. CFD-based analysis of the wall effect on the pressure drop in packed beds with moderate tube/particle diameter ratios in the laminar flow regime. *Chem. Eng. J.* **2009**, *155*, 404–410. [CrossRef]
24. Dasgupta, S.; Atta, A. Analysis of single phase newtonian and non-newtonian velocity distribution in periodic packed beds. *Chem. Eng. J.* **2017**, *324*, 182–193. [CrossRef]
25. Jia, X.; Gui, N.; Yang, X.; Tu, J.; Jia, H.; Jiang, S. Experimental study of flow field characteristics on bed configurations in the pebble bed reactor. *Ann. Nucl. Energy* **2017**, *102*, 1–10. [CrossRef]
26. Chen, L.; Lee, W.; Lee, J. Analysis of the thermal field and heat transfer characteristics of pebble beds packed in a face-centered cubic structure. *Appl. Therm. Eng.* **2017**, *121*, 473–483. [CrossRef]
27. Bu, S.; Li, Z.; Ma, Z.; Sun, W.; Zhang, L.; Chen, D. Numerical study of natural convection effects on effective thermal conductivity in a pebble bed. *Ann. Nucl. Energy* **2020**, *144*, 107524. [CrossRef]
28. Hu, Y.; Yang, J.; Wang, J.; Wang, Q. Investigation of hydrodynamic and heat transfer performances in grille-sphere composite pebble beds with DEM-CFD-Taguchi method. *Energy* **2018**, *155*, 909–920. [CrossRef]
29. Wang, J.; Yang, J.; Cheng, Z.; Liu, Y.; Chen, Y.; Wang, Q. Experimental and numerical study on pressure drop and heat transfer performance of grille-sphere composite structured packed bed. *Appl. Energy* **2018**, *227*, 719–730. [CrossRef]
30. Ferng, Y.M.; Lin, K.-Y. Investigating effects of BCC and FCC arrangements on flow and heat transfer characteristics in pebbles through CFD methodology. *Nucl. Eng. Des.* **2013**, *258*, 66–75. [CrossRef]
31. Song, S.; Cai, X.; Liu, Y.; Wei, Q.; Guo, W. Pore scale thermal hydraulics investigations of molten salt cooled pebble bed high temperature reactor with BCC and FCC configurations. *Sci. Technol. Nucl. Install.* **2014**, *2014*, 1–16. [CrossRef]
32. Dave, A.; Sun, K.; Hu, L. Numerical simulations of molten salt pebble-bed lattices. *Ann. Nucl. Energy* **2018**, *112*, 400–410. [CrossRef]
33. Chen, L.; Lee, J. Effects of inserted sphere on thermal field and heat-transfer characteristics of face-centered-cubic-structured pebble bed. *Appl. Therm. Eng.* **2020**, *172*, 115151. [CrossRef]
34. Bergman, T.; Lavine, A. *Fundamentals of Heat and Mass Transfer*, 8th ed.; Wiley: Hoboken, NJ, USA, 2011.
35. Chen, Y.; Kim, S. *Computation of Turbulent Flows Using an Extended k-Epsilon Turbulence Closure Model*; Interim Report Universities Space Research Association: Columbia, MD, USA, 1987; p. 11969.
36. KTA3102.2 Reactor Core Design of High-Temperature Gas-Cooled Reactors Part 2: Heat Transfer in Spherical Fuel Elements. 1983. Available online: http://www.kta-gs.de/e/standards/3100/3102_2_engl_1983_06.pdf (accessed on 3 November 2021).
37. Yang, G.; Yang, J.; Xu, A. Simulation of convective heat transfer in a packed bed with hexagonal close-packed particles. *J. Wuhan Univ. Sci. Technol.* **2019**, *42*, 314–320. [CrossRef]